JOURNAL OF MATERIALS SCIENCE **35** (2000) 5199–5205

Time resolved USAXS study of the shish–kebab structure in PE: Annealing and melt crystallization

F. ANIA, D. R. RUEDA, F. J. BALTÁ CALLEJA
Instituto de Estructura de la Materia, C.S.I.C., c/Serrano 119, 28006–Madrid, Spain
E-mail: iemd300@csic.es

G. V. KROSIGK
University of Rostock, c.o. DESY/HASYLAB, Notkestr. 85, 22603–Hamburg, Germany

Real time changes in the shish–kebab structure of high molecular weight polyethylene samples, produced by elongational flow injection moulding, were investigated by ultra small angle X–ray scattering (USAXS) using synchrotron radiation. The variation of the two typical long periods has been followed *in situ*, during heating and cooling from the molten state, as a function of temperature and time. Values of the length of the coherently diffracting domains perpendicular to the lamellar stacking planes, as derived from the USAXS maxima, are also presented. Results are discussed in the light of a shish–kebab model in which two different lamellar populations are respectively associated with an epitaxial growth from the columnar shish fibrils and with a secondary lamellar crystallization.

1. Introduction

Elongational flow injection molding is a processing method which produces high strength polymeric materials due to the self reinforcing effect of the highly oriented fibrils [1, 2]. The morphology, often found in these oriented systems, is described as a shish-kebab structure [3, 4]. This morphology was first reported by Pennings and coworkers on rapidly stirring a polyethylene (PE) solution in a subcooled state [5]. Keller and coworkers proved that such a morphology could also be obtained in PE on crystallization from the melt by an extrusion method [6]. The shish–kebab structure consists predominantly of extended chain core crystals along the injection direction, formed by elongational flow, and epitaxially grown stacked lamellae, which appear on cooling.

In a previous paper [7], the changes in the two axial long periods found in injection molded oriented linear PE with a shish-kebab structure were investigated as a function of temperature by ultra–small angle X-ray scattering (USAXS) using synchrotron radiation. For high molecular weight (HMW) oriented PE samples, the initial two long periods $L_1 = 35$ and $L_2 = 66$ nm measured at room temperature, were shown to gradually transform to an apparently single long period at $T = 130^\circ$C. This single long period takes a final value $L_f = 120$ nm at $T = 137^\circ$C. The variation of the long period L_1 with temperature was shown to be independent from the variation of the L_2 periodicity. From these results it was concluded that: 1) The oriented shish-kebab structure consists of two separate populations of lamellar stacks with the layer normals parallel to the injection direction; 2) On heating below $T = 130^\circ$C, only the thinner lamellae thicken till they reach a similar size to the larger ones; 3) On heating at higher temperatures ($T > 130^\circ$C), both populations of lamellae increase further up to $T = 137^\circ$C. At this temperature, the scattering maxima vanish, suggesting the melting of the lamellae. At this point, the oriented fibrils within the HMWPE material still retain their orientation due to the high thermal stability of the shish structure [8]. After cooling, the molten lamellae recrystallize epitaxially on the preserved oriented shish fibrils. Consequently, both stacking periodicities L_2 and L_1 appear again.

The size and distribution of lamellar thicknesses and long periods for the PE mouldings have been also comparatively studied using other techniques such as transmission electron microscopy (TEM) and low frequency Raman spectroscopy [9, 10]. From these studies it was concluded that the length of the straight–chain segments in HMWPE, derived from the Raman bands, agrees well with the double periodicity obtained from USAXS. On the contrary, direct measurements from TEM provide only evidence about the shorter periodicity. However, it is noteworthy that laser light diffraction and Fourier transformation of the same electron micrographs yield two long periods in all regions investigated. A possible explanation for the above discrepancy has been given in terms of the role played by weakly crystalline interlamellar zones which cannot be detected by statistical methods such as Raman or X–ray and light scattering, but that can be individually observed by TEM [10]. The aim of the present study is twofold:

1) To supplement the above investigations throwing light about the origin of the independent variation of

the two long periods during annealing of the highly oriented shish–kebab structure.

2) To examine the dependence of the shish–kebab structure upon crystallization temperature, below the melting point of the epitaxially grown lamellae.

2. Experimental

Samples of high molecular weight linear PE (Lupolen 5661B with $M_w = 190{,}000$ and $\rho = 959$ kg/m^3) were selected for this study. Oriented PE bars with a square cross–section of 4×4 mm were prepared by elongational flow injection molding [11] using a melt temperature of $T_m = 145^\circ$C and a mold temperature of $T_c = 20^\circ$C. The specimens investigated were about 1 mm thick cuts from the inner part of the bars. The ultra–small angle X–ray scattering (USAXS) line BW4 in conjunction with the synchrotron source at the DORIS–bypass (DESY) was used to obtain the SAXS patterns of the oriented PE samples. A two dimensional 512×512 Gabriel detector with a spatial resolution of 0.39 mm per pixel was used. A sample-detector distance of 12.7 m and a wavelength of 0.1381 nm were chosen. The beam path was kept in a vacuum of 10^{-6} mbar. The changes in the SAXS pattern were followed at various temperatures, placing the samples in a hot stage. The samples were positioned with the X–ray beam perpendicular to the injection direction. During the X–ray scattering experiments the specimens were wrapped with aluminium foil to improve the heat exchange and to prevent the flow of material at temperatures approaching the melting point. The heating of the samples was carried out stepwise in the range between room temperature and the melting point at selected temperatures. A heating rate of 10 K/min, allowing the sample to reach the programmed temperature in 1 min before the recording of the SAXS pattern, was used. Exposure times of 5 min were required. PC programs developed at HASYLAB (AIR1 and TOP) were used, respectively, to perform background subtraction and meridional and azimuthal scans of the SAXS maxima. Long periods were calculated from meridional cuts of the original patterns after background subtraction. The position and width at half height of the peak maxima were determined after resolving their separate intensity contributions, which were assumed as simple Gaussian curves.

3. Results

3.1. *In situ* temperature dependence of the long periods

Fig. 1 illustrates the *in situ* measured variation of the two long periodicities as a function of heating temperature. The obtained results are essentially the same as those published in [7] up to 130°C, i.e.: the larger long period $L_2 = 66$ nm remains constant while the smaller one, $L_1 = 36$ nm, increases continuously from room temperature up to a similar value to L_2 at about 130°C. From that temperature upwards both peaks are difficult to separate. However, a careful analysis taking into account the corresponding minimum coherence length values, seems to reveal the occurrence of a cross–over of the position of the intensity maxima while both long periods further increase. This means that the initially shorter spacing, L_1, becomes larger than L_2 at $T > 130^\circ$C. Concurrently, a pronounced decrease of intensity in the meridional scattering is observed. At 135°C only one weak single peak can be resolved (grey shaded circle in the figure). Finally, for temperatures beyond 137°C no traces of meridional scattering were detected, while the equatorial continuous scattering further increases with temperature (see ref. 7).

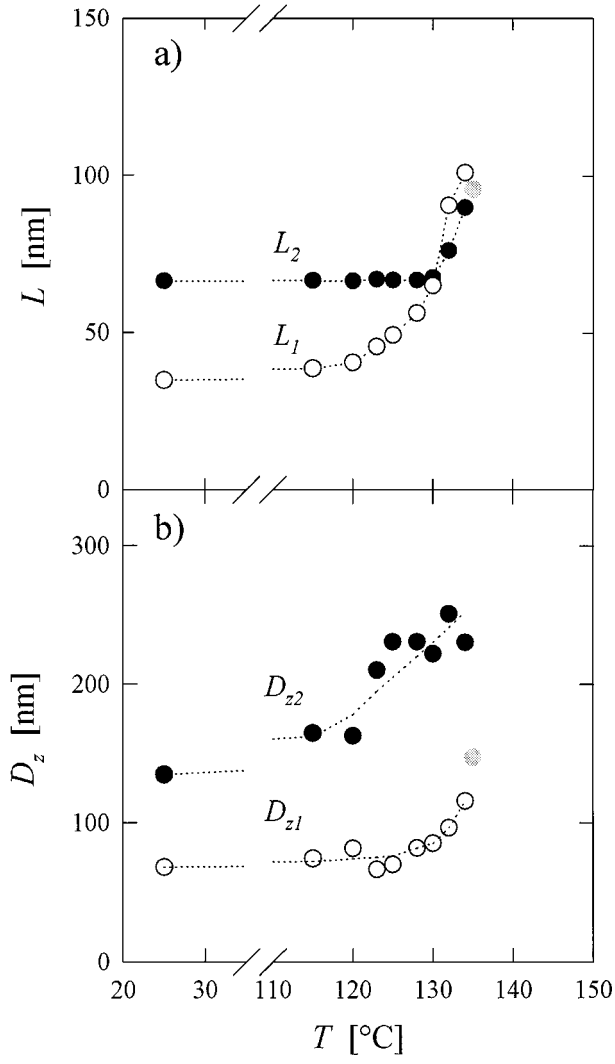

Figure 1 (a) USAXS long period and (b) minimum coherence length in the chain direction for oriented HMWPE as a function of temperature. Solid symbols correspond to the scattered intensity maximum appearing at the lower diffraction angle. At the highest temperature (grey shaded circles) only one maximum could be detected.

Let us consider next the dependence of the coherence length along the fiber direction D_z as a function of temperature (Fig. 1b). The value of D_z has been calculated from the integral width $\delta\beta \sim 1/D_z$ of the two diffraction maxima (L_1 and L_2) of Fig. 1a [12]. This procedure provides a minimum size for the coherently diffracting domains, containing periodic differences in electronic density which arise from the packing of lamellar stacks. It can be observed that the value of D_z continuously increases with temperature up to $T \approx 132^\circ$C for both long periods. These results differ, to some extent, from those previously reported [7] due to the improvement in

the separation of peaks performed in the present study above 130°C.

The obtained results confirm our previous finding concerning the occurrence of two independent populations of lamellar stacks, whose thermal evolution shows a different behaviour: The shorter long period L_1 is capable of increasing its value around three times, while L_2 only changes by about 40%. Simultaneously, the minimum D_z value along the orientation direction similarly increases with temperature for both lamellar populations, being always larger for the longer periodicity.

3.2. Influence of annealing temperature on the long periods measured at room temperature

Most revealing is the comparison of the above results, measured *in situ* at a given temperature, with those measured at room temperature after annealing at similar temperatures. Fig. 2 shows the long period variation after a thermal treatment of $t_a = 30$ min at a given T_a followed by a rapid quenching to room temperature. The measured long periods of Fig. 2 are smaller than those of Fig. 1. This is mainly due to the crystallization, on cooling, of thinner more imperfect crystals, giving rise to smaller average values and, to a lesser extent, to the difference in thermal expansion with temperature. The shorter long period L_1 is practically constant from the initial value at room temperature up to the point corresponding to a thermal treatment at 120°C. Above this temperature, L_1 slightly increases reaching a value of nearly 50 nm at $T \approx 137$°C. From that temperature upwards, the long period decreases to values similar to those measured at room temperature, indicating that the thinner lamellar population has melted and that the annealing effect has been lost. The L_2 values behave in a similar manner, however exhibiting a shift to higher temperatures, i.e.: they remain practically constant up to 135°C and reach a maximum of 80 nm at 139°C. This means that the thicker crystals contributing to the lamellar population L_2 are more stable than those corresponding to L_1.

Aiming to test the effect of a long annealing time, one data point (triangles) corresponding to a material annealed at 135°C for 65 h has also been included. It can be observed that the long period L_1 is lower while L_2 is higher than the corresponding data for $t_a = 30$ min. This result clearly demonstrates the influence of annealing time on the reorganization of the oriented structure of the HMWPE.

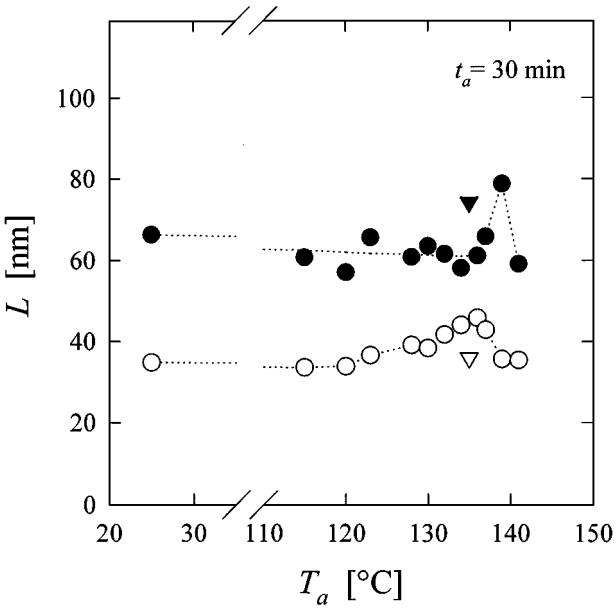

Figure 2 Variation of the long periods of HMWPE, measured at room temperature, after an annealing time of 30 min as a function of annealing temperature. Symbols as in Fig. 1. Triangles correspond to a sample with an annealing time of 65 hours.

3.3. Real time variation of the long periods upon annealing

In order to deepen our knowledge on this matter, the real time dependence of the long spacing (a) and coherence lengths (b) for samples which were annealed at different temperatures (122, 125, 127, 130 and 132°C) was examined (Fig. 3). For the first three temperatures

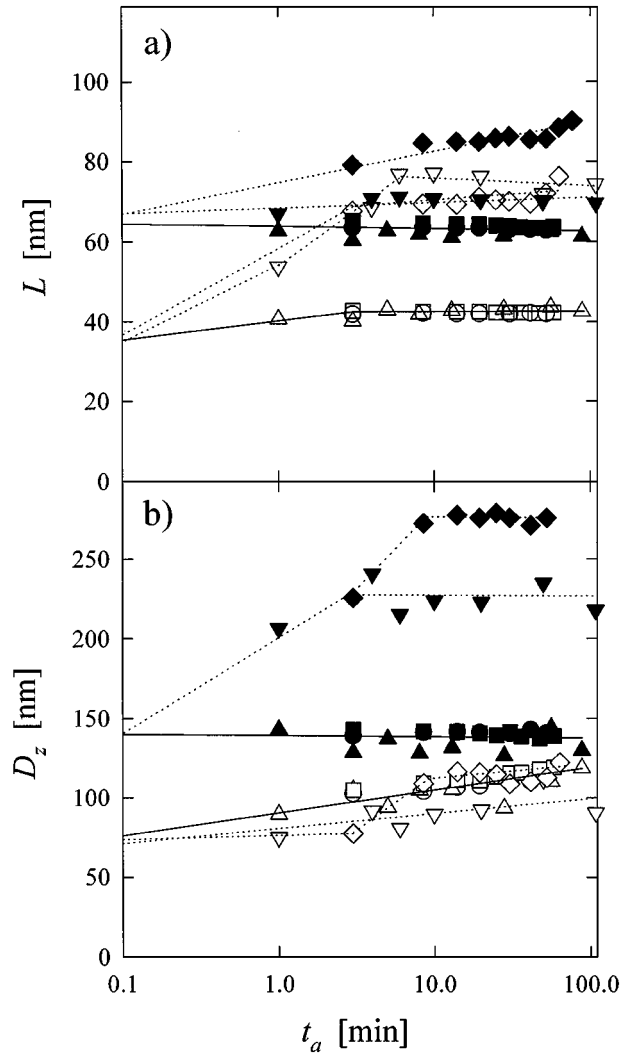

Figure 3 Real time changes of (a) long periods L and (b) coherence lengths D_z for different annealing temperatures: ○ = 122°C, △ = 125°C, □ = 127°C, ▽ = 130°C, ◇ = 132°C. Solid symbols correspond to the scattered intensity maximum appearing at the lower diffraction angle. Solid lines represent the average behaviour at the three lower temperatures.

(122–127°C), very small variations of both long spacing and coherence length values with time are observed (solid lines). This means a slight linear decrease of L_2 and D_{z2} (solid symbols), while L_1 and D_{z1} (open symbols) slightly increase. At 130°C, the shorter long period L_1 strongly increases linearly with the logarithm of time for approximately 6 min and then reaches a constant value of 75 nm. L_2, in turn, linearly increases with log t_a showing final values which are lower than those of L_1 (above mentioned cross–over effect). At 132°C the time variation of L_2 further increases, while that of L_1 increases for about 8 min and then remains constant showing smaller values than L_2. The coherence length corresponding to L_1 has a small linear variation with the logarithm of time for all the investigated temperatures. For L_2, the coherence length remains constant for the three lower temperatures. At 130 and 132°C, a linear increase is observed during the first minutes, followed by a final levelling off.

3.4. Crystallization from the molten state of the lamellae

Complementary information to that presented above is derived from the study of the long period values developing on crystallization from the melt. We understand here by "melt" to be the melting of all the lamellae, which is completed at around 140°C. However at this temperature there are still a number of shish fibrils that survive [7]. Fig. 4 shows the long spacing and the coherence length variation as a function of the crystallization temperature of several samples, measured *in situ* after cooling from the melt. The values were measured once the two long periods were well defined. Their variation with time will be discussed later. The first two points correspond to injection moulded samples having mould temperatures of 20 and 60°C respectively. It is clearly seen that the two long periods are two increasing functions of T_c, which converge towards very similar values above 130°C. The coherence length of the corresponding maxima (Fig. 4b) shows a larger rate of increase with T_c for L_2 than for L_1, similarly to the annealing data depicted in Fig. 3. If one assumes, as a first approximation, that the two–phase model applies to our lamellar system, one can write: $l_i = L_i w_{ci}$, where L_i ($i = 1, 2$) is the long period, l_i the crystal thickness of the lamellae and w_{ci} the degree of crystallinity for each data point. Thomson–Gibbs equation could then be rewritten as:

$$L = \frac{2T_m^0 \sigma_e}{\Delta T \Delta h^0 w_c} \qquad (1)$$

where $\Delta T = T_m^0 - T_m$ is the supercooling and T_m^0, the thermodynamic melting point of an infinitely thick crystal [13]. Accordingly we can replot the long spacings of Fig. 4a as a function of the reciprocal of the supercooling ΔT (Fig. 5). Thomson's equation defines a linear function when plotting crystal thickness l_i against $1/\Delta T$. We have used the following values for PE: $T_m^0 = 415$ K, fold surface free energy $\sigma_e = 7.0 \times 10^{-2}$ J m^{-2} and enthalpy of fusion $\Delta h^0 = 2.82 \times 10^8$ J m^{-3}

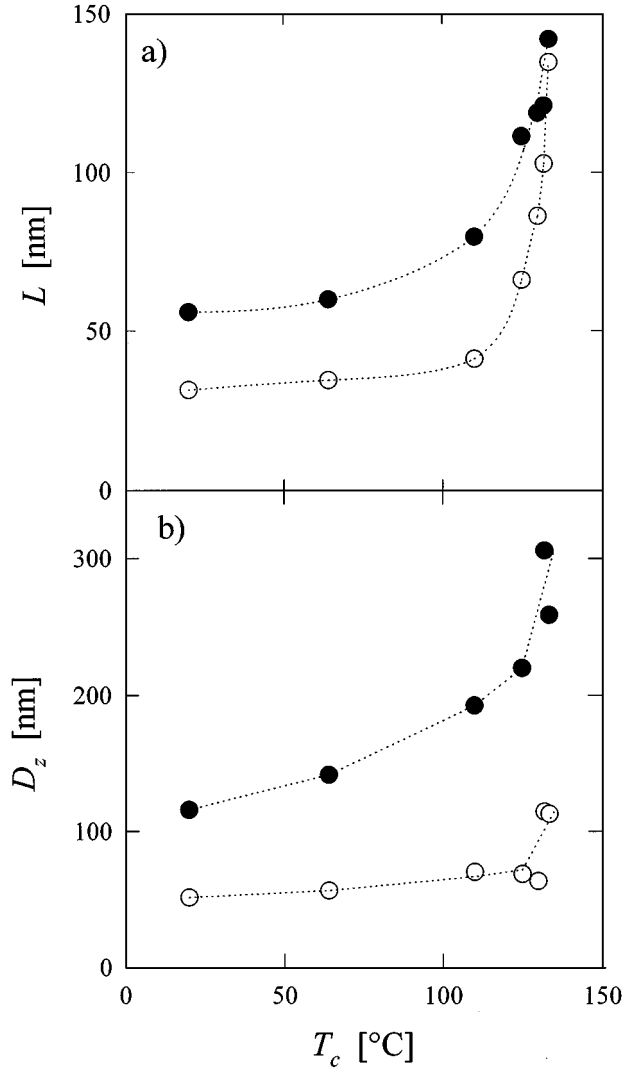

Figure 4 Long period L (a) and coherence length (b) corresponding to various crystallization temperatures T_c. Symbols as in Fig. 1.

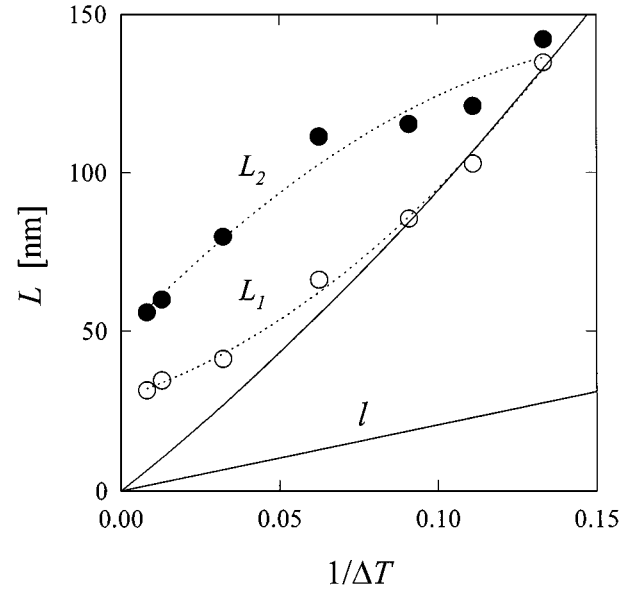

Figure 5 Same long period data as in Fig. 4 plotted as a function of the reciprocal value of the supercooling $\Delta T = T_m^0 - T_m$. The straight line represents the variation of crystal thickness l according to Thomson–Gibbs equation. The continuous curve shows the estimated behaviour of long spacing L.

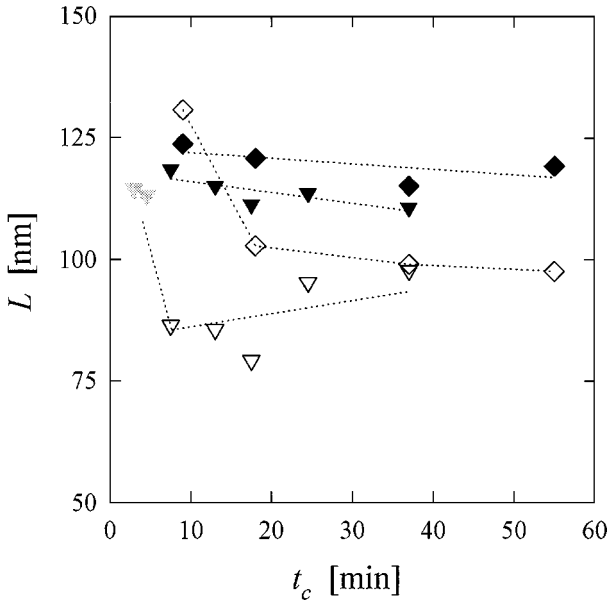

Figure 6 Real time variation of the long periods for two crystallization temperatures: $\triangledown = 130^\circ$C, $\diamond = 132^\circ$C. Solid symbols correspond to the scattered intensity maximum appearing at the lower diffraction angle. Points shaded in gray denote that the scattering intensity could not be resolved into two maxima.

[13]. However, the plot of L_i should deviate from linearity because crystallinity w_{ci} is a decreasing function of supercooling. The straight line in Fig. 5 represents the predicted variation of l according to Equation 1, whereas the continuous curve illustrates the estimated behaviour of L imposed by the fit of data for the lowest supercoolings.

Finally, as mentioned above, the long spacings appearing on crystallization from the melt do not remain constant with time. Fig. 6 illustrates the long spacing variation with time of the USAXS maxima at two given crystallization temperatures (130 and 132°C). While L_2 does not seem to change much at both temperatures, showing only a small decrease with time, L_1 strongly decreases for short crystallization times. The L_1 decrease, which amounts to about 30%, occurs sooner for the lowest temperature investigated. After this, a further slight decrease is observed for $T_c = 132^\circ$C while for $T_c = 130^\circ$C, a tendency to increase seems to occur. The latter might be related to concurrent annealing of the crystallized material.

4. Discussion

As starting model for the discussion of results we adopt an interpenetrating shish–kebab morphology [4] composed of two independent populations of lamellae, as supported in previous studies [7, 9]. All experiments, described so far, support the different time and/or temperature dependence of the two periodicities L_1 and L_2, which (with the only exception of small intervals of temperatures very close to melting upon annealing or crystallization) are always well resolved. A reasonable hypothesis referring to the latter point could be that the lamellae appearing first (responsible for L_2) are those which grow epitaxially from the extended shish fibrils at the early stages of crystallization. These dominant lamellae should not have any spacial constraint. The remaining crystallizable material would give rise to secondary thinner lamellae which, at a later stage, give rise to shorter long periods (L_1). The latter can be envisaged as a secondary crystallization within the liquid domains which were not filled by the initial kebabs. Keller [6] proposed a further growth of the initial lamellae at the lamellae tips tending towards a well developed interpenetration between lamellar kebabs of adjacent shish columns. Let us next discuss our experimental data in the light of the above structural model.

4.1. Annealing behaviour

Figs 1–3 have several points in common: The first one is the independent evolution of the two long periods, both as a function of temperature and heating time. The shorter long spacing L_1 shows a more pronounced variation than L_2. This could be explained by the fact that the corresponding lamellae are thinner and less stable than those of L_2. Thus, on thermal treatment, L_1 undergoes reorganization at lower temperatures and shorter heating times in contrast with L_2. On the other hand, the D_z values increase due to the thermal treatment (Fig. 1b). However, the increase in coherence length of the crystals occurs, this time, at lower temperatures for the thicker lamellae than for the thinner ones. At the highest T_a used, D_{z2} improves much more its minimum coherence length than D_{z1} (Fig. 3b). This means that from the viewpoint of regularity of the scattering repeating distance, it is easier for the longer periodicities to reorganize. This could be explained by the fact that the lamellar population providing shorter long periods is constrained to certain domains where, in spite of being able to recrystallize into longer spacings, the initial coherence length cannot improve so easily.

4.2. Crystallization from the melt

The plot of the long spacings as a function of degree of supercooling ΔT in Fig. 5 shows a remarkable deviation of the fitted experimental curves (dotted curves) from the expected behaviour (continuous curve). L_2 values are always higher than those calculated because, according to our model, epitaxial growth from the shish columns rapidly starts at very small supercoolings. Crystallization then takes place long before the nominal crystallization temperature is reached producing, as a result, much larger crystal thicknesses and long spacings. The initial long spacing, appearing at low ΔT, gradually decreases with increasing ΔT owing to a subsequent secondary crystallization. On cooling, new more imperfect lamellae appear upon crystallization of the molten material, filling the gaps between the dominant primary lamellae. In contrast to L_2, the shorter long spacing values L_1 start to deviate from the continuous line at higher supercoolings because many of these lamellae are probably formed during secondary crystallization.

Most revealing is the time evolution of the long spacings L_2 and L_1 investigated at 130 and 132°C (Fig. 6). For these high crystallization temperatures neither of

the periodicities can be resolved during the first 5 min of crystallization. At 132°C, L_2 and L_1 have very similar initial values due to the free growth of both lamellar types. At a later crystallization time, both periodicities are well separated showing higher values the higher T_c. L_2 values only diminish slightly because the corresponding lamellae have been formed already and do not change any more. On the contrary, L_1 values abruptly fall for both crystallization temperatures (somewhat faster for the lower temperature). This suggests that crystallization proceeds, occurring at a faster rate at the lower temperature. The insertion of new thin lamellae among the initial ones could be responsible for such a decrease of L_1. The final increase of L_1 at $T_c = 130°C$ should be related, as mentioned above, with annealing of the crystallized material which is most displaced from thermodynamic equilibrium.

A sketch of the proposed model for the two existing lamellar populations within the shish–kebab structure, at two different temperatures, is shown in Fig. 7. Fig 7a shows the initial two periodicities at room temperature: one corresponding only to distances among kebab primary lamellae epitaxially grown from the shish cores, while the other one arises from the repeating distance among kebabs and secondary lamellae. These secondary lamellae are also oriented because their growth is probably influenced by the surrounding primary lamellae (kebabs) and by the remaining memory of the initial elongational flow.The model includes the possibility of several lamellae merging so close to each other that they create a unique area of high electron density. This feature could be identified with the weakly crystalline interlamellar zones which have been directly observed by TEM [10]. It is evident that the model oversimplifies a very complex system, where two types of domains, including lamellae of a single average crystal size (dual lamellar stack model as opposed to the depicted bimodal domains), cannot be ruled out [7, 14].

A temperature increase up to about 132°C would lead to the structure represented in Fig. 7b. Here the thinner lamellae are molten and the remaining ones are thicker due to the annealing effect. The resulting long periods have very similar values at this temperature. It is noteworthy that according to Figs 1 and 4 the evolution of the two long periods and their corresponding minimum coherence length follows very similar paths on heating from room temperature and on recrystallizing from the lamellar melt. Reversibility is not fully accomplished due to the fact that all these processes are kinetically controlled and time effects are usually very important (Fig. 6) [15].

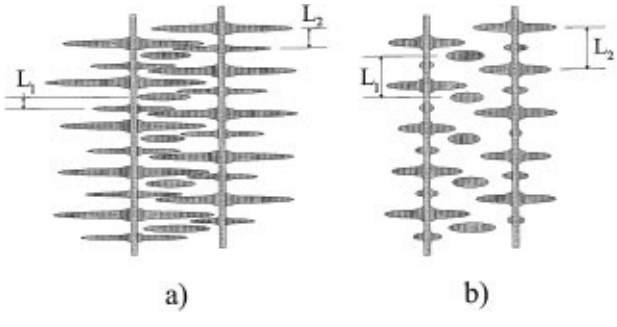

Figure 7 Schematic view of the shish–kebab structure at two different temperatures: (a) room temperature and (b) ∼132°C. The two long periodicities L_1 and L_2 are indicated.

5. Conclusions

1) The X–ray long periodicities of oriented PE with a shish–kebab structure and the corresponding coherently diffracting domains in chain direction have been studied as a function of both annealing time and temperature and crystallization time and temperature.

2) The two long periods show an independent behaviour from each other, which is mainly a function of temperature and, to a minor extent, of annealing time.

3) From the above findings, a structural model which confirms the existence of two separate lamellar populations is proposed. Accordingly, upon melt crystallization at a given temperature the population of primary lamellae, epitaxially growing from the persistent shish fibrils, appears first. The thinner secondary lamellae are inserted at a later stage within the former ones.

4) The more pronounced variation of L_1 values as compared with L_2, has been associated with the higher reorganization capability of the secondary lamellae. Notwithstanding, this reorganization seems to be spatially restricted by the surrounding primary lamellae as revealed by the observed smaller changes of the coherence length D_{z1} along the fiber direction.

Acknowledgements

We wish to thank Dr. R. K. Bayer, Kassel, for the preparation and kind supply of the investigated samples, Dr. U. Lode for software development and Ms. Sabine Cunis (HASYLAB) for technical assistance. The work was supported by DGICYT, Spain (Grant PB94–0049). USAXS measurements at the DORIS–bypass, DESY, Hamburg, have been funded by the TMR–Contract ERBFMGECT950059 of the European Community.

References

1. R. K. BAYER, A. E. ELIAH and J. C. SEFERIS, *Polym. Eng. Rev.* **4** (1984) 201.
2. G. W. EHRENSTEIN and C. MAERTIN, *Kunststoffe* **75** (1985) 105.
3. A. J. PENNINGS, R. LAGEVEEN and R. S. DE VRIES, *Coll. Polym. Sci.* **255** (1977) 532.
4. Z. BASHIR, J. A. ODELL and A. KELLER, *J. Mater. Sci.* **21** (1986) 3993.
5. A. J. PENNINGS and A. M. KIEL, *Kolloid–Z.* **205** (1965) 160.
6. J. A. ODELL, D. T. GRUBB and A. KELLER, *Polymer* **19** (1978) 617.
7. D. R. RUEDA, F. ANIA and F. J. BALTÁ CALLEJA, *ibid.* **38** (1997) 2027.
8. D. R. RUEDA, F. ANIA, E. LÓPEZ-CABARCOS, F. J. BALTÁ CALLEJA, H. G. ZACHMANN and R. K. BAYER, *Polymers for Adv. Technologies* **2** (1991) 57.
9. F. ANIA, F. J. BALTÁ CALLEJA, R. K. BAYER, A. TSHMEL, I. NAUMANN and G. H. MICHLER, *J. Mater. Sci.* **31** (1996) 4199.
10. G. H. MICHLER, I. NAUMANN, F. J. BALTÁ CALLEJA and F. ANIA, *Acta Polymer.* **48** (1997) 36.

11. R. K. BAYER, F. J. BALTÁ CALLEJA, E. LÓPEZ-CABARCOS, H. G. ZACHMANN, A. PAULSEN, F. BRÜNNING and W. MEINS, *J. Mater. Sci.* **24** (1989) 2643.
12. F. J. BALTÁ CALLEJA and C. G. VONK, "X-ray Scattering of Synthetic Polymers" (Elsevier, Amsterdam, 1989).
13. B. WUNDERLICH, "Macromolecular Physics, Vol. 2" (Academic Press, New York, 1976).
14. R. K. VERMA and B. S. HSIAO, *TRIP* **4** (1996) 312.
15. G. STROBL, "The Physics of Polymers" (Springer–Verlag, Berlin, 1997).

Received 1 March
and accepted 2 March 2000